https://doi.org/10.1016/j.ijmecsci.2016.09.013

Evaluation for tool flank wear and its influences on surface roughness in ultra-precision raster fly cutting

Guoqing Zhang[a,b*], Suet To[b,c], Shaojian Zhang[b]

[a] Guangdong Provincial Key Laboratory of Micro/Nano Optomechatronics Engineering, College of Mechatronics and Control Engineering, Shenzhen University, Nan-hai Ave 3688, Shenzhen 518060, Guangdong, PR China

[b]State Key Laboratory of Ultra-precision Machining Technology, Department of Industrial and Systems Engineering, The Hong Kong Polytechnic University, Kowloon, Hong Kong, PR China

[c]Shenzhen Research Institute of The Hong Kong Polytechnic University, Shenzhen 518060, Guangdong, PR China

* Corresponding Author / E-mail: sandy.to@polyu.edu.hk, Tel: +852-2766-6587, Fax: +852-2764-7657

Abstract: The occurrence of tool flank wear certainly affects the machined surface roughness in ultra-precision machining. The in-process evaluation of tool flank wear and its effects on machined surface roughness is significant, since it helps to find tool flank wear timely and reduce tool wear effect on surface roughness by further actions. However, little attention has been paid to the evaluation of tool flank wear and its effects on machined surface roughness in ultra-precision raster fly-cutting (UPRFC) process especially by using cutting chips. In the present research, evaluation of tool flank wear and its effects on surface roughness is conducted in UPRFC by examination of cutting chip morphologies. Based on the relations between chip morphologies and tool flank wear, a mathematical model was established to identify the width of flank wear land and the theoretical surface roughness under tool flank wear effects. Theoretical and experimental results show that: (1) Tool flank wear occurrence causes the formation of shutter-like structure rather than feather-like structure at the tool entry of cutting chips. (2) Cutting chips are truncated where chip thickness is comparable to the width of wear land. (3) The smooth tool flank wear increase the tool nose radius and therefore reduce the surface toughness theorectically.

Keywords: Diamond tool; Tool wear; Cutting chips; Ultra-precision raster fly cutting; Surface roughness

1. Introduction

In ultra-precision machining, tool wear affects the surface roughness [1], chip formation [2], cutting force [3], even chatter stability [4] and delamination [5]. Therefore, the in-process evaluation of tool wear and its effects on surface roughness is quite important, since it can detect the poor surface quality caused by tool wear timely, avoid unacceptable cutting and even remedy the surface deterioration. Up to date, research about the evaluation of tool wear has been focused on conventional machining, single point diamond turning, micro milling and conventional drilling process both in direct and indirect methods. Direct tool wear evaluation methods are usually performed by optical inspection. Some typical examples are: Sortino, et al., (2003)

adopted a method of statistical filtering for optical detection of tool wear [6]. Wang, et al., (2006) utilized direct optical methods to measure the flank wear of diamond tools [7]. Li, et al., (2013) developed a novel online optical system to inspect and measure tool wear conditions in milling [8]. However, the optical inspection of tool wear is difficult to be realized in-process since diamond tools are covered by chips during cutting process. Therefore, many indirect tool wear evaluation methods were adopted, such as evaluation of tool wear by using cutting force, acoustic emission, power consumption, and even vibration signals. for example, Emel and Kannatey-Asibu, (1989) employed an acoustic emission and force-based sensor fusion system involving pattern recognition analysis to detect tool breakage, chip formation and a threshold level of tool flank wear in turning [9]. Lin, et al., (1995) utilized force signals to achieve on-line drill wear monitoring [10]. Salgado, et al., (2007) presented a tool condition monitoring system (TCMS) for on-line tool wear monitoring in turning by using the feed motor current and the sound signal [11]. Alonso, et al., (2008) developed a reliable tool condition monitoring system (TCMS) based on the analysis of structure of tool vibration signals [12]. The indirect signals can reflect the gradually wear of cutting tools, however there is no accurate indirect tool wear evaluation methods for industrial application.

Surface quality evaluation is another essential topic in ultra-precision machining, a significant body of research has been focused on it. For example, Cheung and Lee, (2001) conducted a study about the characterization of nano-surface generation in single-point diamond turning [13]. Their following work focused on the effect of tool interference on surface generation in single-point diamond turning [14]. Quinsat et al., (2008) proposed a 3D surface roughness parameter which can formalize the relative influence of both machining parameters and surface requirements in ball end milling process [15]. Ahn, et al., (2009) presented an elaborate methodology to predict the surface roughness of layered manufacturing processed parts [16]. Also, many attempts were employed to realize online surface quality prediction. For example, Singh, et al.,(2004) revealed a new methodology for predicting surface roughness of engineering surfaces based on the acoustic characterization [17]. Grzesik and Brol, (2009) characterized the surface profiles generated in longitudinal turning operations using continuous wavelet transform [18]. Karayel, (2009) presented a neural network approach for the prediction and control of surface roughness in a computer numerically controlled (CNC) lathe [19]. In addition, Kılıçkap, et al., (2005) conducted a research on the relationship between tool wear and surface roughness in machining of homogenized SiC-p reinforced aluminum metal matrix composite [20]. However, no research was reported on the in-process evaluation of tool wear effects on machined surface quality, especially in ultra-precision raster fly-cutting (UPRFC) process.

UPRFC is a typical intermittent cutting process, the relative complex cutting mechanism of UPRFC makes the in-process evaluation of tool wear and its effect on surface quality difficult, because the diamond tool is rotating in high speed during the UPRFC. Most of research about surface generation in UPRFC has been reported under the consideration of cutting parameters [21-22], cutting strategy [23], kinematics error [24], spindle vibration [25] and workpiece materials [26]. For tool wear characteristics and their effects on machined surface roughness, Yin, et al., (2009) was among the first to investigate the tool wear characteristics in UPRFC [27]. Afterwards, Zhang, et al., (2015) conducted a research to further investigate tool wear characteristics in UPRFC and their effect on cutting force, chip morphology and surface finish [28]. Our previous study focused on the evaluation methods of tool fractures and their effects on surface roughness by using cutting chips [29-30]. Moreover, the relation between tool flank wear and chip morphology was preliminarily investigated [31]. However, surface quality evaluation under the consideration of tool flank wear of diamond tools has not been reported in UPRFC, especially for in-process evaluation and using cutting chips.

In the present research, an in-process evaluation method for tool flank wear and its effects on surface roughness was employed by examining cutting chips. The effective of this method is based on the typical intermittent cutting mechanism of UPRFC. In this method, the cutting chips were collected in a certain interval time. The collected cutting chips were then examined by SEM, the inspected results were used to identify the width of flank wear land. The machined surface roughness under tool wear effect can also be predicted based on the tool flank wear identification. This method can realize the in-process evaluation of tool flank wear and its effects on machined surface roughness. Based on the evaluation, the machined surface quality can be potentially improved by optimizing cutting parameters.

2. Experiments

In this investigation, the cutting experiment was performed on a Precitech 705G ultra-precision raster fly cutting machine which owns five axes including three translation axes (*X*, *Y*, *Z*) and two rotatable axes (*B*, *C*). The experimental setup is shown in Fig. 1. The workpiece material used in the cutting experiment was brass material. Cutting parameters are listed in Table 1. In the experiment, a desired flat cutting and depth cutting were performed. The total cutting distance was about 5000m. The total cutting time was about 450h.

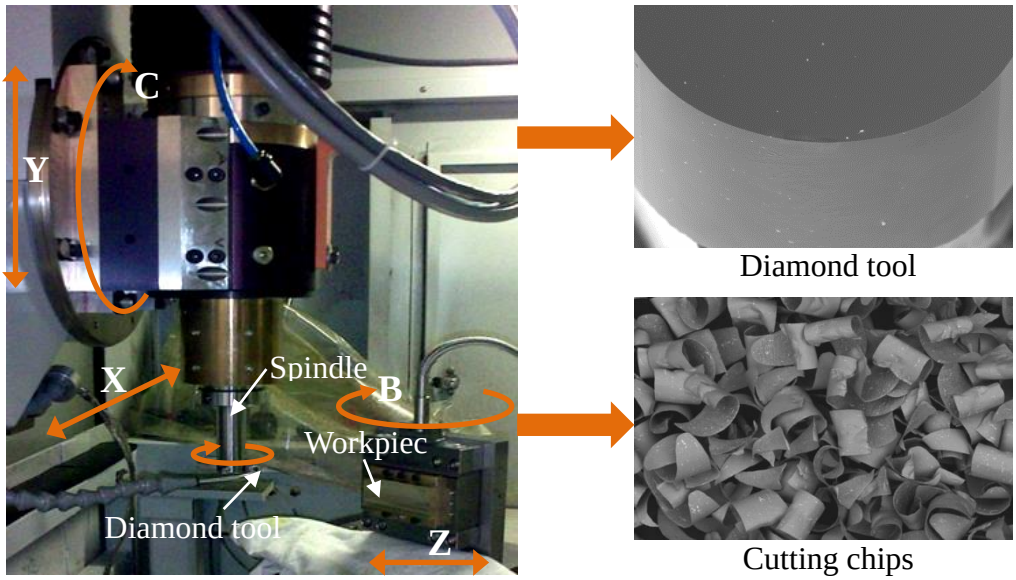

Fig.1 Experimental setup

Before the flat cutting and after every 1000m flat cutting, a group of depth cutting was conducted to investigate the effect of wear land on the cutting chips morphology. The cutting depths in the depth cutting were 2μm, 5μm, 10μm and 15μm respectively. The cutting parameters for flat cutting and depth cutting are listed in the second and third columns of table 1 respectively.

Table 1 Cutting conditions in flat cutting and depth cutting

Items	**Flat cutting**	**Depth cutting**
Tool type	Insert diamond tool(Apex Inc.)	
Rake angle	-2.5°	
Clearance angle	15°	
Tool radius	0.631mm	
Feed rate	200mm/min	225mm/min
Step distance	0.025mm	0.025mm
Spindle speed	4500 rpm	4500 rpm
Depth of cut	0.03mm	2μm,5μm,10μm, 15μm
Swing distance	28.35mm	28.35mm
Cutting strategy	Horizontal cutting	Horizontal cutting
Cutting environment	Lubricant on	Lubricant on

To compare the morphologies of cutting chips cut by a fresh tool and a worn tool, cutting chips were collected at the first stage of the cutting experiment and at the end of every 1000m flat cutting and every depth cutting. The collected chips were then examined by Hitachi TM3000 scanning electron microscope (SEM). After finishing every 1000m of flat cutting, the diamond tool was dismounted and then inspected by the

Hitachi TM3000 SEM. After cutting, a Park's XE-70 atomic force microscope (AFM) was used to measure the wear land angle.

3. Results and discussion

In UPRFC, the contact between cutting tool and workpiece in a rotary cutting circle is quite short, which can be proved by the form of the captured cutting force as shown in Fig.2. The short cutting duration make the cutting tool suffering the effect of cyclical stress. Therefore, the tool wear characteristics in UPRFC are different from that in continuous cutting process.

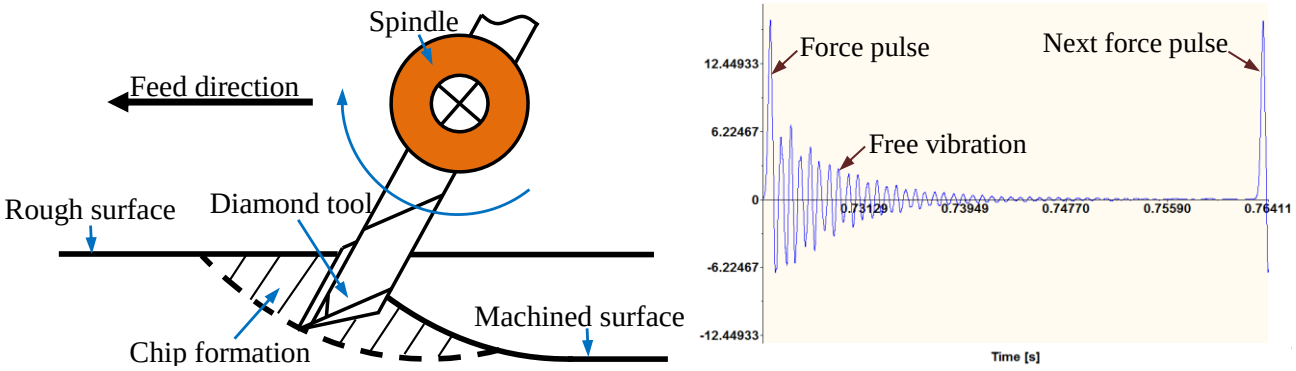

Fig. 2 Cutting mechanism illustration of UPRFC and its cutting force forms

Fig.3 shows the tool wear characteristics at different cutting stages. It is found from Fig.3 (a) that fresh diamond tool usually owns sharp cutting edge. After about 1000m flat cutting, some fractures were found on the cutting edge, the bigger ones of which are marked by F_1 and F_2 in Fig.3 (b). After 2000m flat cutting, it is found from Fig.3 (c) that the two bigger fractures were flatten a little. Fig.3 (d) shows the tool figure after 3000m flat cutting. It is found that the cutting edge is not sharp any more, instead, a round cutting edge is formed. In addition, the two bigger fractures are flatten a lot. Fig.3 (e) indicates the diamond tool figures after a 4000m flat cutting, it is found that a smooth wear land is formed, the width of the wear land is in the range of 0.5-1um. Also it is found that the two bigger fractures are flatten and hard to be distinguished. Fig.3 (f) shows the SEM tool wear figure after a 5000m flat cutting. It is found that the tool wear pattern has no significant difference from that shown in Fig.3 (e), only the width of wear land has a little increase.

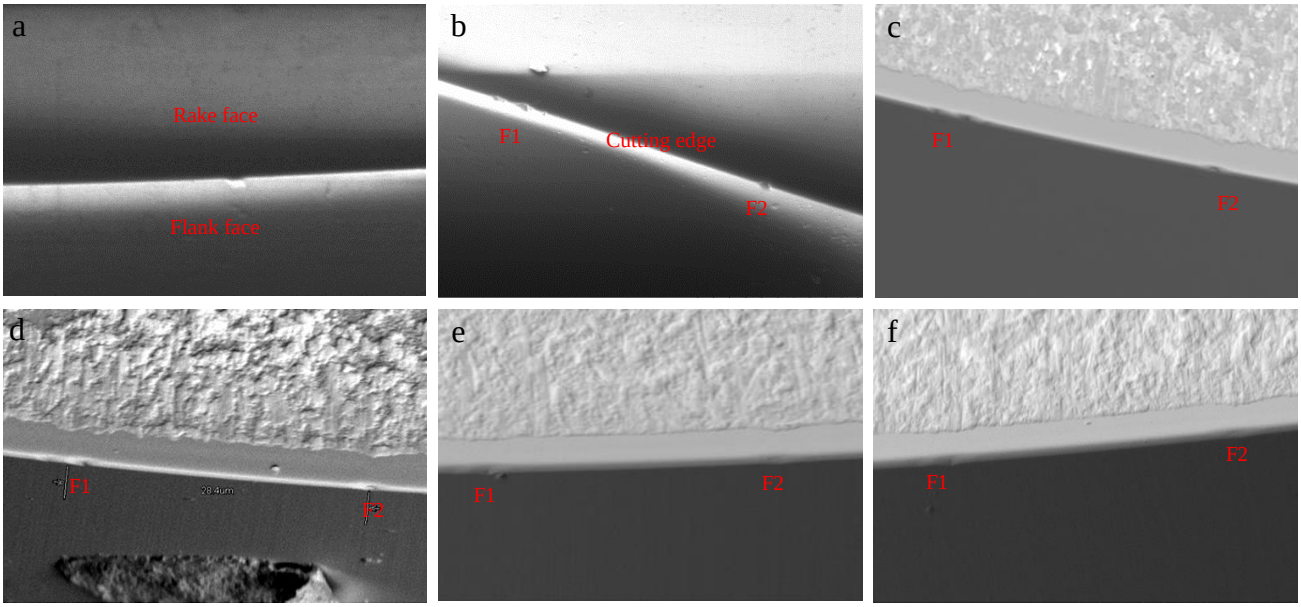

Fig. 3 SEM photographs of cutting tool edge of (a) a fresh tool and worn tool at the cutting distance about (b) 1000 m, (c) 2000 m, (d) 3000 m, (e) 4000 m and (f) 5000 m

The occurrence of tool wear certainly affects the cutting chip morphology. Fig. 4 (a) shows the morphology of a cutting chip cut by a fresh tool, it is found that the cutting chip is quite thin at its tool entry, some feather-like structure are formed. While Fig. 4(b) shows the morphology of a cutting chip cut by a tool after 5000m flat cutting. It is found the cutting chip is truncated, some shutter-like structures are formed at its tool entry side.

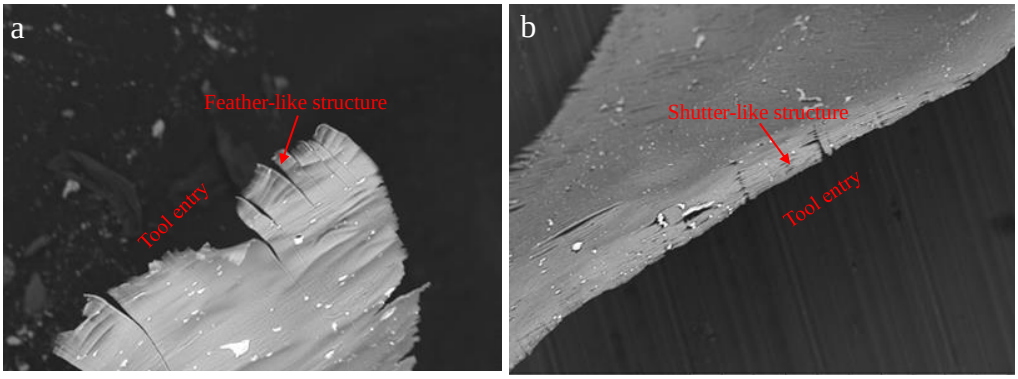

Fig. 4 SEM figures of cutting chips at the cutting distance about (a) 3.6m and (b) 5000m

The shutter-like structure is caused by the formation of smooth wear land. With the progress of the tool flank wear, as the cutting edge radius of a diamond tool is comparable to the thickness of cutting chips, a macro cutting instead of micro cutting process occurs. This will lead to the formation of some gaps in the lamella structure, so that a shutter-like structure is formed.

Before cutting and after each 1000 m flat cutting, a group depth cutting is performed with the cutting

depth of 2μm, 5μm, 10μm, and 15μm respectively. In each depth cutting, the cutting chips were collected. Fig. 5 shows the figures of cutting chips cut by the fresh tool at different cutting depth, it is found that all the cutting chips can be fully generated at different cutting depth.

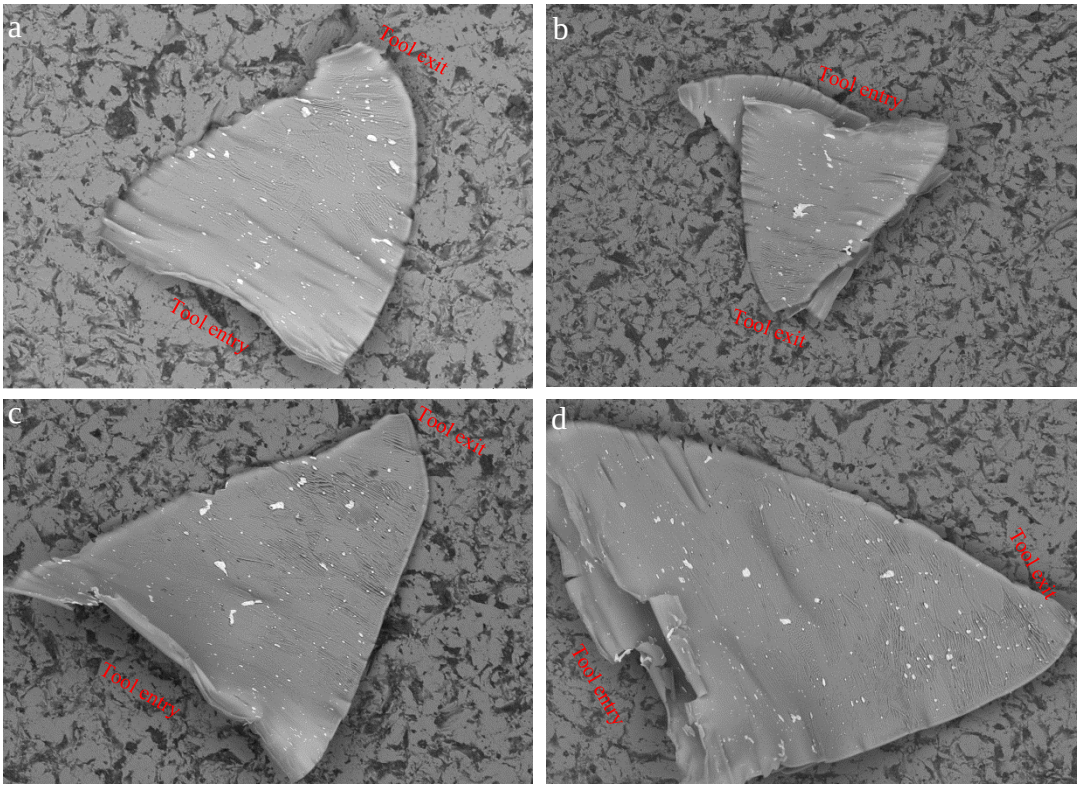

Fig.5 Cutting chips cut by a fresh tool at the cutting depth of (a) 2μm, (b) 5μm, (c) 10μm and (d) 15μm

Fig.6 shows the figure of cutting chips cut by a worn tool at different cutting depth. From these figures, it is found that the cutting chips have different morphologies at the different cutting depth. At the cutting depth of 2μm, the cutting chips can not be formed, only some needle-like structures were found, as is shown in Fig.6 (a). At the cutting depth of 5 μm, some chips were formed, however the chip is truncated on both their tool entry and tool exit sides. The chip truncation occurs perpendicular to the cutting direction, which makes cutting chips incomplete (see Fig.6 (b)). At the cutting depth of 10μm and 15μm, although the chip trunction still ocurred, the truncated area is seriously decreased as comparing to that at the cutting depth at 5μm.

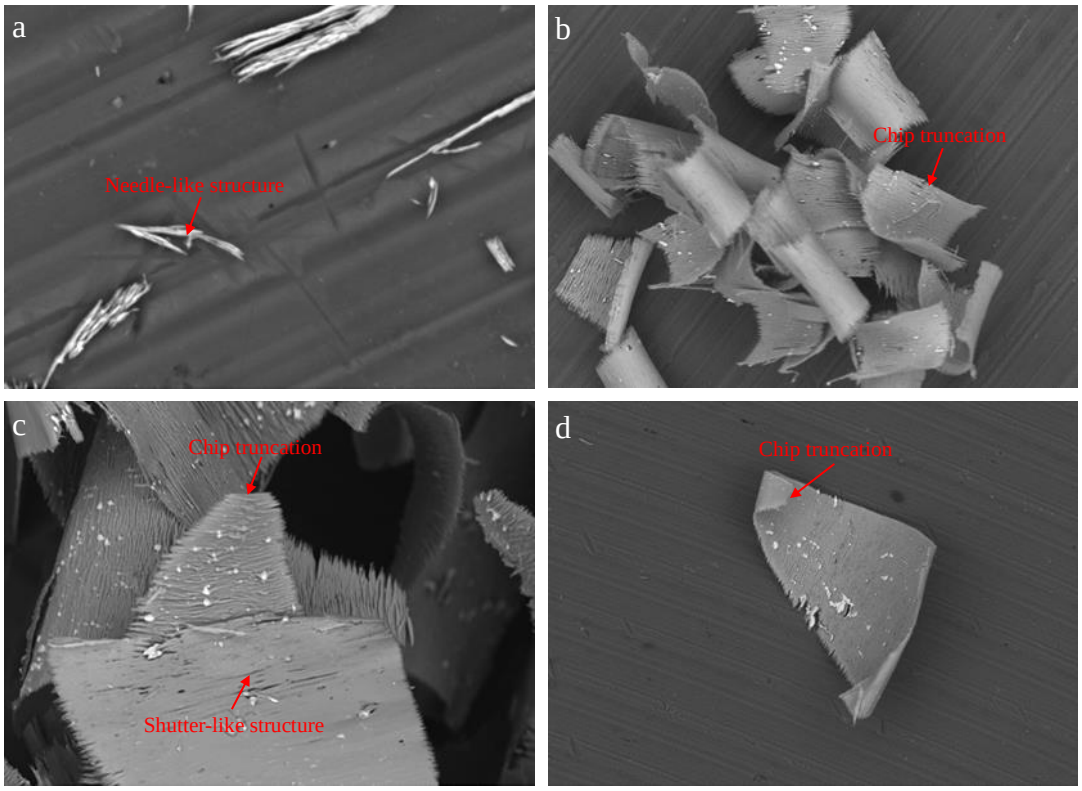

Fig. 6 Cutting chips cut by the worn tool at the cutting depth of (a) 2μm (b) 5μm (c) 10μm (d) 15μm

Since the truncation of cutting chips was also found at other cutting distances, it is evident that this truncation was caused by the tool flank wear. For a cutting tool, there is a corresponding critical chip thickness (CCT) in the feed direction of cutting chips. As the cutting depth is smaller than the CCT, the cutting tool cannot cut down any materials from the workpiece and the cutting chips cannot be generated.

4. Mathematical model

Fig.7 shows the schematic of cutting mechanism and chip formation in UPRFC process. Due to the intermittent cutting property of UPRFC, the cutting chip is fully generated in a rotary cutting. In the UPRFC process, the diamond tool rotates around the spindle axis cutting into and out of the machined surface intermittently. Since UPRFC is a rotary fly cutting of diamond tool with an arc cutting edge, the tool imprints left on the machined surface are torus. Chips are generated as a result of three cutting steps in a rotary cutting: previous step cutting, previous rotary cutting and current rotary cutting, as is schematic illustrated in Fig.7 (a-b). Correspondingly, cutting chips are enveloped by four surfaces: the rough surface (R_s), the surfaces formed by previous rotary cutting (P_r), current rotary cutting (C_r), and previous step cutting (P_s), as is shown in Fig.7(c).

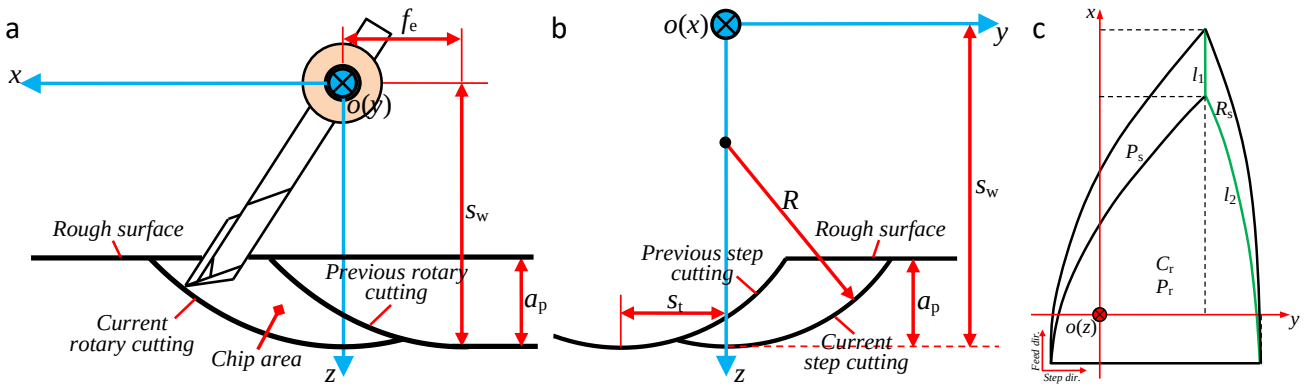

Fig. 7 Schematic of cutting mechanism of UPRFC in a (a) side view and (b) back view, and (c) chip formation

Therefore, a mathematical model is established to simulate the 3D cutting chip morphology, as is listed in Eqs. (1). Since the cutting chip is enveloped by four surfaces, Eqs. (1) are composed of four equations and each of them depicts one surface.

$$\begin{cases} \left(\sqrt{\left(x+f_e\right)^2+z^2}-s_w+R\right)^2+y^2=R^2 \\ \left(\sqrt{x^2+z^2}-s_w+R\right)^2+y^2=R^2 \\ \left(z-s_w+R\right)^2+\left(y+s_t\right)^2=R^2 \\ z=s_w-a_p \end{cases} \tag{1}$$

Where s_w is the swing distance of cutting tools; s_t is the step distance; R is the tool nose radius; a_p is the cutting depth; f_e is the feed rate.

The origin and geometric meaning for each equation in Eqs.(1) are listed in table 2.

Table 2 Equations for chip surfaces

Surfaces	Equations	Geometric shape
P_r	$\left(\sqrt{\left(x+f_e\right)^2+z^2}-s_w+R\right)^2+y^2=R^2$	Torus
C_r	$\left(\sqrt{x^2+z^2}-s_w+R\right)^2+y^2=R^2$	Torus
P_s	$\left(z-s_w+R\right)^2+\left(y+s_t\right)^2=R^2$	Cylindrical surface
R_s	$z=s_w-a_p$	Plane

Based on the mathematical model of cutting chip, the simulated cutting chip morphology and its profile in other three orthogonal views are shown in Fig.8. From Fig.8, it is found that the cutting chip morphology is

a leaf-like structure with thicker thickness at its central position while thinner at its two sides along the cutting direction.

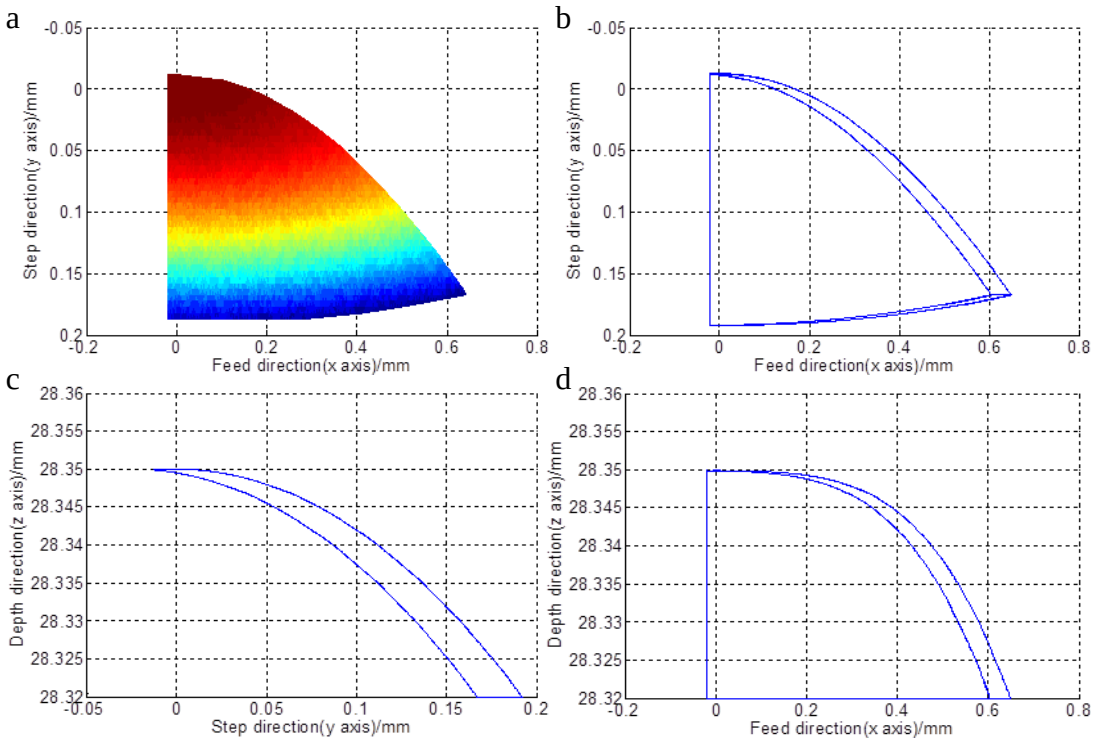

Fig.8 (a) Simulated cutting chip morphology and its profile in a (b) top view, (c) back view and (d) side view

Since the truncation position of cutting chips is sensitive to the distance along the feed direction of cutting chips, in this research, the chip thickness curve with respect to the distance in the chip length direction is modeled as:

$$C_t = \sqrt{(x_1 - x_0)^2 + (y_1 - y_0)^2 + (z_1 - z_0)^2} \tag{2}$$

Where C_t denotes the chip thickness, x_0, y_0, z_0 are the coordinate components of the points on the line l_1 and l_2 (see Fig.7(c))of cutting chips, expressed as:

For line l_1, it is the boundary curve of surface P_s and R_s, combining their equations and eliminating z, given by:

$$\begin{cases} x_m \le x_0 \le x_k \\ y_0 = \sqrt{a_p(2R - a_p)} - s_t \\ z_0 = s_w - a_p \end{cases} \tag{3}$$

For line l_2, it is the boundary curve of surface P_r and R_s, combining their equations and eliminating z, yields:

$$\begin{cases} x_0 = \sqrt{(\sqrt{R^2 - y^2} + s_w - R)^2 - (s_w - a_p)^2} - f_e \\ \sqrt{a_p(2R - a_p)} - s_t \le y_0 \le \sqrt{R^2 - (\sqrt{f_e^2/4 + (s_w - a_p)^2} - s_w + R)^2} \\ z_0 = s_w - a_p \end{cases} \tag{4}$$

Corresponding to x_0, y_0, z_0, x_1, y_1, z_1 are the coordinate components of the points on back face of cutting chips. They are the intersection point between the back face of the cutting chips and the line connecting the original point of coordinate system *o-xyz* and point x_0, y_0, z_0, given by:

$$\begin{cases} x_1 = \dfrac{x_0(s_w - R)\sqrt{x_0^2 + z_0^2} \pm x_0\sqrt{R^2(x_0^2 + z_0^2) - y_0^2 s_w(s_w - 2R)}}{x_0^2 + y_0^2 + z_0^2} \\ y_1 = \dfrac{y_0(s_w - R)\sqrt{x_0^2 + z_0^2} \pm y_0\sqrt{R^2(x_0^2 + z_0^2) - y_0^2 s_w(s_w - 2R)}}{x_0^2 + y_0^2 + z_0^2} \\ z_1 = \dfrac{z_0(s_w - R)\sqrt{x_0^2 + z_0^2} \pm z_0\sqrt{R^2(x_0^2 + z_0^2) - y_0^2 s_w(s_w - 2R)}}{x_0^2 + y_0^2 + z_0^2} \end{cases} \tag{5}$$

Based on the Eq.(2), the chip thickness curve is plotted in Fig.9.

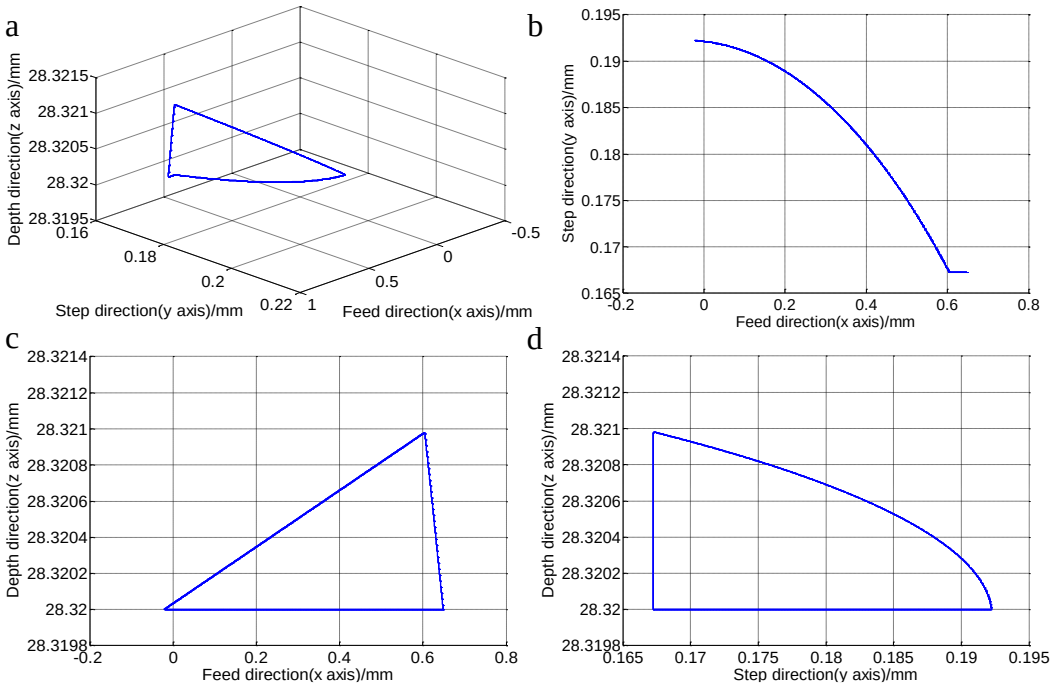

Fig.9 The chip thickness curve (a) in axis-equal view, (b) in side view, (c) with respect to the distance in the feed direction and (d) in back view

From Fig.9 (a) it is found that the chip thickness curve is a spatial curve, while its three views are shown in Fig.9 (b-d). From Fig.9 (c), it is found that the chip thickness increase from zero to the maximum and then

decrease to zero again along its length direction. Therefore, the shape of cutting chip is thicker at its central place while thinner at its two sides. This geometric shape of cutting chips makes it suitable to identify the tool flank wear. Based on the 'minimum cutting depth theorem', in the chip formation by using a worn tool, part of the cutting chip cannot be generated at which the chip thickness less than the height of wear land. Therefore, the CCT can reflect the wear land height and even wear land width since the cutting chip will be truncated at a chip thickness comparable to the height of wear land. There is a correspondence between the CCT and the height of wear land, although the correspondence relation between the CCT and wear land height is not very accurate.

To identify the CCT at the chip truncation position, two methods can be used. In the first method, the width of cutting chips at their truncation position was used to identify the CCT based on the Fig.10 (a). Another method is based on the length of truncated cutting chips, as is shown in Fig.10 (b). However, due to the compression effect during the cutting, the cutting chip length in simulated and actual is different, to reflect the compression effect on the cutting chip morphology, the simulated cutting chip length should be corrected to fulfil the actual length of cutting chips.

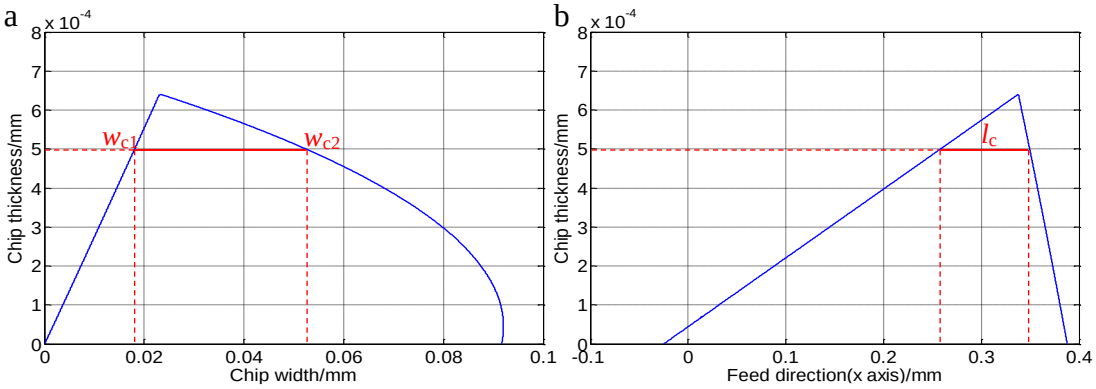

Fig.10 Two methods used to identify the chip thickness: (a) chip width method at the truncation position (b) chip length method

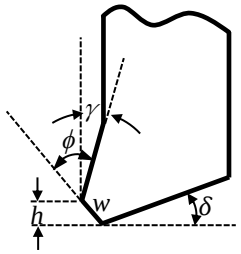

Fig.11 Geometric relation for wear land width and wear land height

After identification of the mean value of identified CCTs, the wear land height (h) can also be known.

For simplicity, we make the wear land height equal to the CCT. Therefore, based on geometric relations in Fig.11, the wear land width can be calculated by the wear land angle and wear land height, given by:

$$w = h / \cos(\phi + \gamma) \tag{6}$$

Where w is the width of wear land; h is the height of the wear land, which is equal to the CCT; ϕ is the wear land angle, according to the AFM measurement result as shown in Fig.12, ϕ is 40.5° for brass material; γ is the rake angle of diamond tool, in this investigation γ=-2.5°.

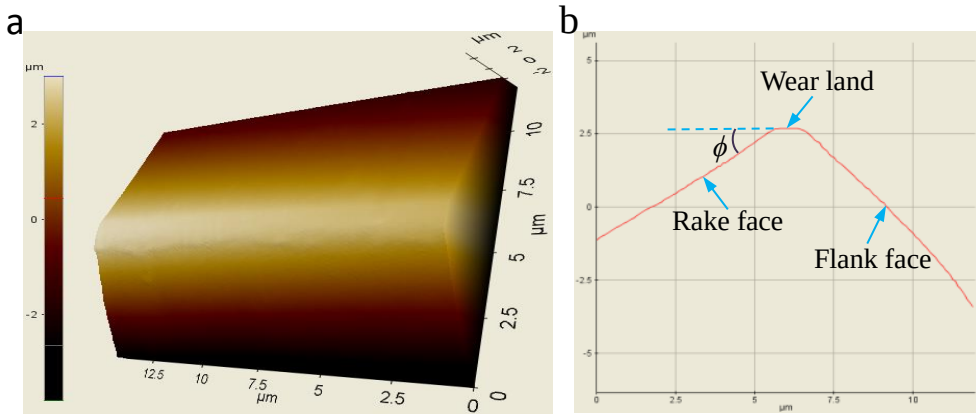

Fig.12 (a) Cutting edge photo measured by Atomic Force Microscope (Park's XE-70) and (b) the measured sectional profile curve of cutting edge

5. Tool flank wear influences on the surface roughness

The occurrence of flank wear of a diamond tool makes its cutting edge retracted and leads to the formation of a new cutting edge. Fig.13 shows the schematic illustration of cutting edge retraction and their effects on theoretical surface roughness. For simplicity, suppose the new formed cutting edge profile is an arc, the largest deviation between the original cutting edge arc and newly formed cutting edge arc is at the central position of the arc, as is shown in Fig.13 (b). From Fig.13 (b), it is found that the newly formed cutting edge arc owns relative larger tool nose radius and a different arc center.

5.1 Cutting edge retraction

As we know, the surface topography is formed by the imprints of cutting edge, as shown in Fig. 13(c). In the surface topography forming process, the intersection point of two original cutting edges is point *g*. However, the retraction of the cutting edge due to tool flank wear leads to the new intersection between the original cutting edge and worn cutting edge, the intersection point has been changed into point *u*, this behavior will cause a motion of the intersection point. Actually, the retraction of cutting edge and the motion of

intersection point are progressing simultaneously. Therefore, the retraction of cutting edge leads to the intersection of worn cutting edge at point *u*. Due to the bigger cutting edge radius of worn cutting edge, the imprints of the worn cutting edge on the machined surface will cause to a smaller surface roughness, as is shown in Fig.13 (d).

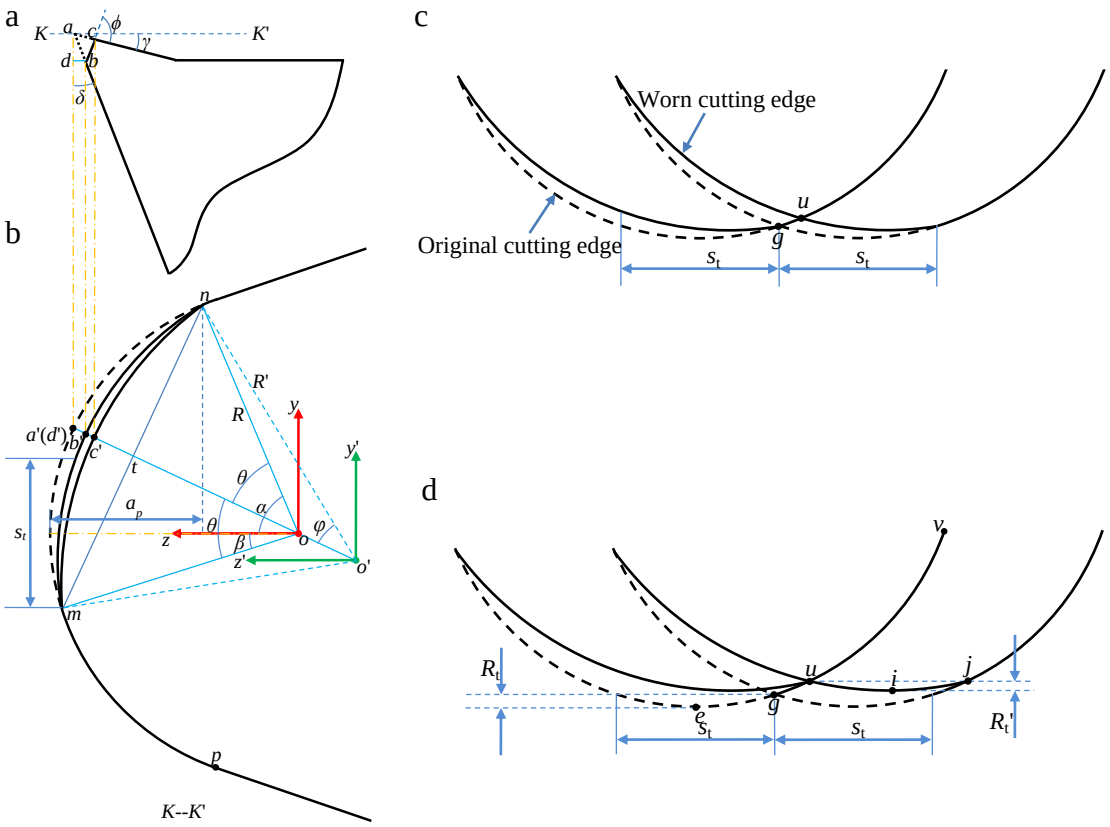

Fig.13 Schematic illustration of the side view (a) and the top view(K--K' plane) (b) of tool flank wear, and the effect of tool flank wear on the surface roughness(c)(d)

For clarity, two coordinate systems *o*-*yz* and *o*'-*y*'*z*' were established to present different arcs, as shown in Fig.13 (b). In Fig.13 (a), $|bc|$ is the wear land width, whose value can be identified from the cutting chips. ϕ is the wear land angle, whose value is 40.5°as brass material being cut.

Based on the geometric relationship, the cutting edge retraction ($|bd|$) can be calculated from the Sine law. As is shown in Fig.13 (a), in triangle Δabc, $\angle \mathrm{acb} = \phi$, $\angle bac = 90° - \delta - \gamma$, according to the Sine law:

$$\frac{|bc|}{\sin(90^\circ - \delta - \gamma)} = \frac{|ab|}{\sin\phi} \tag{7}$$

From Eq.(7), the length $|ab|$ can be calculated as:

$$|ab| = \frac{\sin\phi}{\sin(90^\circ - \delta - \gamma)}|bc| = \frac{\sin\phi}{\sin(90^\circ - \delta - \gamma)}w \tag{8}$$

Where *w* is the wear land width.

In triangle Δabd, the length $|bd|$ can be calculated as:

$$|bd| = |ab| \sin\delta = \frac{\sin\phi \sin\delta}{\sin(90^\circ - \delta - \gamma)} w \tag{9}$$

In mapping plane *K*-*K*', cutting edge retraction $h_l = |b'd'|$, we obtain:

$$h_l = |b'd'| = |bd| = \frac{\sin\phi \sin\delta}{\sin(90^\circ - \delta - \gamma)} w \tag{10}$$

5.2 New formed tool nose radius

The tool flank wear in the UPRFC process makes the tool material loss-zone a crescent-like profile that is thicker at the center position while thinner at two sides, as is shown in Fig.13 (b). Suppose the newly formed cutting edge and the original cutting edge are intersected at the point *m* and *n*, while the central point of new cutting edge arc *mn* is *b*'.

In Fig.13(b), based on the geometric relationship and cutting parameters, we obtain:

$$\begin{cases} \cos\alpha = \left(R - a_p\right)/R \\ \sin\beta = \dfrac{s_t}{2R} \end{cases} \tag{11}$$

From Eqs.(11), two angle α and β can be calculated as:

$$\begin{cases} \alpha = \arccos\left(\dfrac{R - a_p}{R}\right) \\ \beta = \arcsin\left(\dfrac{s_t}{2R}\right) \end{cases} \tag{12}$$

Therefore, θ in Fig.13(b) can be calculated as:

$$\theta = \frac{\alpha + \beta}{2} \tag{13}$$

In triangle *ont* in Fig.13(b), $|nt|$ can be solved as:

$$|nt| = R\sin\theta \tag{14}$$

Similarly, in triangle of *o'nt*, $\sin\varphi$ is calculated as:

$$\sin\varphi = \frac{|nt|}{R'} = \frac{R\sin\theta}{R'} \tag{15}$$

From Eq.(15), the angle of φ can be computed as:

$$\varphi = \arcsin\left(\frac{R\sin\theta}{R'}\right) \tag{16}$$

Since the difference of $|d't|$ and $|b't|$ equals to the height of the loss zone (h_l), yields:

$$(R - R\cos\theta) + (R' - R'\cos\varphi) = h_l \tag{17}$$

Submitting Eq.(16) into φ in Eq.(17), yields:

$$R(1-\cos\theta) - R'\left[1-\cos\left(\arcsin\left(\frac{R\sin\theta}{R'}\right)\right)\right] = h_l \tag{18}$$

Eq.(18) can also be written as a function as:

$$F(R') = R(1-\cos\theta) - R'\left[1-\cos\left(\arcsin\left(\frac{R\sin\theta}{R'}\right)\right)\right] - h_l = 0 \tag{19}$$

From Eq.(19), R' can be solved from numerical method.

The theoretical peak-to-valley roughness in UPRFC is calculated as[30]:

$$\begin{cases} R_{t\_\min} = R_{t\_tool} = R - \sqrt{R^2 - (s_t/2)^2} \\ R_{t\_\max} = R_{t\_swing} + R_{t\_tool}/\cos\alpha = s_w - \sqrt{s_w^2 - (f_e/2)^2} + \dfrac{s_w\left(R - \sqrt{R^2 - (s_t/2)^2}\right)}{\sqrt{s_w^2 - (f_e/2)^2}} \end{cases} \tag{20}$$

As the tool flank wear occurs, a new tool nose radius(R') is formed, the theoretical peak-to-valley roughness is changed into:

$$\begin{cases} R'_{t\_\min} = R' - \sqrt{R'^2 - (s_t/2)^2} \\ R'_{t\_\max} = s_w - \sqrt{s_w^2 - (f_e/2)^2} + \dfrac{s_w\left(R' - \sqrt{R'^2 - (s_t/2)^2}\right)}{\sqrt{s_w^2 - (f_e/2)^2}} \end{cases} \tag{21}$$

5.3 Evaluation system for tool flank wear and its effects on machined surface roughness

The relation between chip morphology and tool flank wear talked above can be used to evaluate the tool flank wear and the surface roughness under flank wear effect. Fig.14 shows the framework of a tool flank wear and its effects on surface roughness in-process evaluation system based on cutting chips. Based on Fig.14, the procedures for in-process evaluation for tool flank wear and its effects on surface roughness are: (1) Collection of cutting chips online without stop cutting process. (2) Examining the cutting chip morphologies, if the cutting chip is truncated, calculation the CCT of cutting chips at their truncated position. (3) Calculation of the wear land width of cutting tools. (4) Calculating the new formed tool nose radius. (5) Calculating the surface roughness R_t based on the worn cutting edge.

In this system, based on the cutting chips model and the examined cutting chip morphology, the tool

flank wear can be evaluated, and a newly formed tool nose radius can be identified. The identified tool nosed radius of the worn tool was then used to predict the machined surface roughness together with cutting parameters. Based on the predicted machined surface quality, some actions can be conducted to improve the deteriorated surface quality. These actions include changing cutting parameters and correction of the tool geometry parameters.

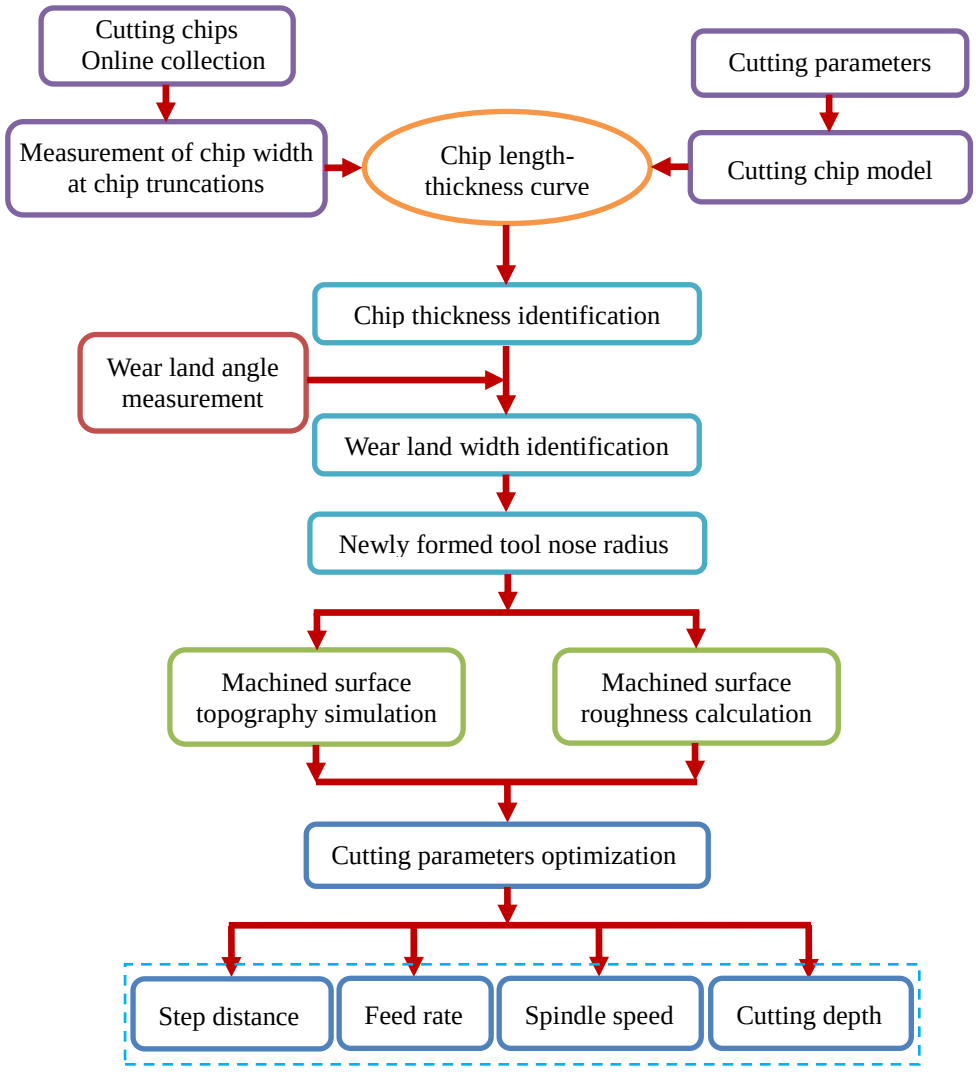

Fig.14 Flowchart of tool flank wear evaluation system based on cutting chips

Following the procedures above, the tool wear evaluation method based on cutting chip morphology can not only realize the identification of tool flank wear but also identify the surface roughness under the effect of tool flank wear without need to stop the cutting machine. Therefore, the evaluation methods addressed in this paper is a promising method for the evaluation of tool flank wear and its effects on surface roughness.

6 Conclusions

In the present research, based on the fact that tool flank wear makes cutting chips truncated at their tool

entry and tool exit sides, a novel in-process evaluation method for tool flank wear and its effects on machined surface roughness in ultra-precision raster fly-cutting (UPRFC) is introduced. Specific conclusions drawn from the study are:

(1) Fresh cutting edge leads to the formation of a feather-like structure at the tool entry of cutting chips, while tool flank wear causes shutter-like structure and even makes the cutting chips truncated at both their tool entry and tool exit sides. Chip truncation direction is perpendicular to the cutting direction, the chip truncation position depends on the chip thickness.

(2) The width of wear land can be identified by using both the length of truncated cutting chip and the width of cutting chips at their truncation position. Due to the existence of material compression during the chip forming process, the length of truncated cutting chips should be corrected first before the identification of tool flank wear.

(3) Tool flank wear causes a newly formed tool nose arc with a relative larger radius and a changed arc center. The retraction of the cutting edge reduces the machined surface roughness theoretically.

(4) A tool condition evaluation system based on the morphology of cutting chips is established, this system can be used to evaluate tool flank wear and even instruct to reduce the effects of tool flank wear on machined surface roughness.

Acknowledgement

This project were supported by the National Natural Science Foundation of China (Grant No. 51505297 and 51275434) and Natural Science Foundation of SZU (Grant No. 2016038).

References:

[1]. Özel T, Karpat Y. Predictive modeling of surface roughness and tool wear in hard turning using regression and neural networks. Int J Mach Tools Manuf 2005; 45(4): 467-479.

[2]. Zhang G, To S, Xiao G. The relation between chip morphology and tool wear in ultra-precision raster milling. Int J Mach Tools Manuf 2014; 80–81:11–17.

[3]. Oraby SE, Hayhurst DR. Development of models for tool wear force relationships in metal cutting. Int J Mach Sci 1991; 33(2): 125-138.

[4]. Chiou YS, Chung ES, Liang SY. Analysis of tool wear effect on chatter stability in turning. Int J Mach Sci 1995; 37(4):391-404.

[5]. Tsao CC, Hocheng H. Effect of tool wear on delamination in drilling composite materials. Int J Mach Sci 2007; 49(8): 983-988.

[6]. Sortino M. Application of statistical filtering for optical detection of tool wear. Int J Mach Tools Manuf 2003; 43(5):493–497.

[7]. Wang WH, Wong YS, Hong GS. 3D measurement of crater wear by phase shifting method. Wear 2006; 261(2):164-171.
[8]. Li W, Singh HM, Guo YB. An online optical system for inspecting tool condition in milling of H13 tool steel and IN 718 alloy. Int J Adv Manuf Technol 2013; 67(5-8):1067-1077.
[9]. Emel E, Kannatey-Asibu E. Acoustic emission and force sensor fusion for monitoring the cutting process. Int J Mach Sci 1989; 31(11–12):795-809.
[10]. Lin SC, Ting CJ. Tool wear monitoring in drilling using force signals. Wear 1995; 180(1-2):53-60.
[11]. Salgado DR, Alonso FJ. An approach based on current and sound signals for in-process tool wear monitoring. Int J Mach Tools Manuf 2007; 47(14):2140–2152.
[12]. Alonso FJ, Salgado DR. Analysis of the structure of vibration signals for tool wear detection. Mech Syst Signal Pr 2008; 22(3):735-748.
[13]. Cheung CF, Lee WB. Characterization of nanosurface generation in single-point diamond turning. Int J Mach Tools Manuf 2001; 41(6):851–875.
[14]. Cheung CF, Lee WB. Prediction of the effect of tool interference on surface generation in single-point diamond turning. Int J Adv Manuf Technol 2002; 19(4):245-252.
[15]. Quinsat Y, Sabourin L, Lartigue C. Surface topography in ball end milling process description of a 3D surface roughness parameter. J Mater Process Technol 2008; 195(1-3):135-143.
[16]. Ahn D, Kim H, Lee S. Surface roughness prediction using measured data and interpolation in layered manufacturing. J Mater Process Technol 2009; 209(2):664-671.
[17]. Singh SK, Srinivasan K, Chakraborty D. Acoustic characterization and prediction of surface roughness. J Mater Process Technol 2004; 152(2):127-130.
[18]. Grzesik W, Brol S. Wavelet and fractal approach to surface roughness characterization after finish turning of different workpiece materials. J Mater Process Technol 2009; 209(5):2522-2531.
[19]. Karayel D. Prediction and control of surface roughness in CNC lathe using artificial neural network. J Mater Process Technol 2009; 209(7):3125-3137.
[20]. Kılıçkap E, Çakır O, Aksoy M, İnan A. Study of tool wear and surface roughness in machining of homogenised SiC-p reinforced aluminum metal matrix composite. J Mater Process Technol 2005; 164–165(15):862-867.
[21]. Wang SJ, Chen X, To S, Ouyang XB, Liu Q, Liu JW, Lee WB. Effect of cutting parameters on heat generation in ultra-precision milling of aluminum alloy 6061. Int J Adv Manuf Technol 2015; 80(5):1265-1275.
[22]. Cheng MN, Cheung CF, Lee WB, To S, Kong LB. Theoretical and experimental analysis of nano-surface generation in ultra-precision raster milling. Int J Mach Tools Manuf 2008; 48(10):1090-1102.
[23]. Wang SJ, To S, Chen X, Chen XD, Ouyang XB. An integrated optimization of cutting parameters and tool path generation in ultra-precision raster milling. Int J Adv Manuf Technol 2014; 75(9-12):1711-1721.
[24]. Kong LB, Cheung CF, To S, Lee WB. An investigation into surface generation in ultra-precision raster milling. J Mater Process Technol 2009; 209:4178-4185.
[25]. Zhang SJ, To S. The effects of spindle vibration on surface generation in ultra-precision raster milling. Int J Mach Tools Manuf 2013; 71:52-56.
[26]. Wang SJ, To S, Cheung CF. An investigation into material-induced surface roughness in ultra-precision milling. Int J Adv Manuf Technol 2013; 68:607–616.
[27]. Yin ZQ, To S, Lee WB. Wear characteristics of diamond tool in ultra-precision raster milling. Int J Adv Manuf Technol 2009; 44(7-8):638-647.
[28]. Zhang G, To S, Zhang S. Relationships of tool wear characteristics to cutting mechanics, chip formation, and surface quality in ultra-precision fly cutting. Int J Adv Manuf Technol 2016; 83(1):133-144.
[29]. Zhang G, To S, Xiao G. Novel tool wear monitoring method in ultra-precision raster milling using cutting chips.

Precis Eng 2014; 38(3):555–560.

[30]. Zhang G, To S. A novel surface quality evaluation method in ultra-precision raster milling using cutting chips. J Mater Process Technol 2015; 219:328–338.

[31]. Zhang G, To S, Xiao G. The relation between chip morphology and tool wear in ultra-precision raster milling. Int J Mach Tools Manuf 2014; 80-81:11-17.